IN-32

JPL PUBLICATION 86-8 (MSAT-X REPORT No. 129)

46 pages

IN-14300

Trellis Coded Modulation for 4800 to 9600 bps Transmission Over a Fading Satellite Channel

Dariush Divsalar
Marvin K. Simon

June 1, 1986

NASA
National Aeronautics and Space Administration

Jet Propulsion Laboratory
California Institute of Technology
Pasadena, California

JPL PUBLICATION 86-8 (MSAT-X REPORT No. 129)

Trellis Coded Modulation for 4800 to 9600 bps Transmission Over a Fading Satellite Channel

Dariush Divsalar
Marvin K. Simon

June 1, 1986

National Aeronautics and
Space Administration

Jet Propulsion Laboratory
California Institute of Technology
Pasadena, California

The research described in this publication was carried out by the Jet Propulsion Laboratory, California Institute of Technology, under a contract with the National Aeronautics and Space Administration.

Abstract

The combination of trellis coding and multiple phase-shift-keyed (MPSK) signaling with the addition of asymmetry to the signal set is discussed with regard to its suitability as a modulation/coding scheme for the fading mobile satellite channel. For MPSK, introducing nonuniformity (asymmetry) into the spacing between signal points in the constellation buys a further improvement in performance over that achievable with trellis coded symmetric MPSK, all this without increasing the average or peak power, or changing the bandwidth constraints imposed on the system.

Whereas previous contributions have considered the performance of trellis coded modulation transmitted over an additive white Gaussian noise (AWGN) channel, the emphasis in this paper is on the performance of trellis coded MPSK in the fading environment. The results will be obtained by using a combination of analysis and simulation. It will be assumed that the effect of the fading on the phase of the received signal is fully compensated for either by tracking it with some form of phase-locked loop or with pilot tone calibration techniques. Thus, our results will reflect only the degradation due to the effect of the fading on the amplitude of the received signal. Also, we shall consider only the case where interleaving/deinterleaving is employed to further combat the fading. This allows for considerable simplification of the analysis and is of great practical interest. Finally, the impact of the availability of channel state information on average bit error probability performance is assessed.

CONTENTS

Figures

Table

SECTION I
INTRODUCTION

There is a growing need for reliable transmission of high-quality voice and digital data in satellite-based land mobile communication systems. These systems, which will be part of an emerging all-digital network, are both power and bandwidth limited. To satisfy the bandwidth limitation, one can employ bandwidth-efficient modulation techniques such as those that have been developed over the past several years for terrestrial microwave communications systems. Examples of these are multiple phase-shift keying (MPSK), quadrature amplitude modulation (QAM) and the various forms of continuous phase frequency modulation (CPM). When power is limited, forward error correction (FEC) coding is ordinarily used.

When both limitations are imposed simultaneously, as in the mobile satellite application, it is most often not possible to achieve the desired throughput with either technique acting alone. Instead, what is required is the integration of a bandwidth-efficient modulation scheme with some form of FEC coding to exploit the best possible attributes of both.

In the past, coding and modulation were treated as separate operations with regard to overall system design. In particular, most earlier works on coded digital communication systems independently optimized: (a) conventional (block or convolutional) coding with maximized minimum Hamming distance, and (b) conventional modulation with maximally separated signals.

About a decade ago, using random coding bound arguments, it was shown that considerable performance improvement could be obtained by treating coding and modulation as a single entity [1]. Many years later, this concept was formalized into a rigorous theory which showed that optimally designed rate $n/(n+1)$ trellis codes suitably mapped (to maximize Euclidean distance) into conventional 2^{n+1}-point signal sets can provide significant coding gain without bandwidth expansion when compared with uncoded conventional 2^n-point signal sets [2]. It is this work that has laid the foundation for the design

and development of all power and bandwidth-efficient digital modems found in practice today and those that are to come in the future.

The most common application of such trellis coded modulation (TCM) techniques is in the new generation of modems being developed for the telephone channel. Indeed, the present state of the art is a rate 6/7, 8-state trellis coded 128-point QAM which is capable of transmitting 14.4 kbps (2.4 ksps) over good-quality (D1-conditioned or better) leased telephone lines [3].

Thus, if it is practical to send 14.4 kbps over the telephone channel, transmitting 4.8 or 9.6 kbps information over a 5-kHz satellite channel (typical of present considerations) might appear to be simple.

Several reasons make this supposition untrue, most of which relate to the additional sources of degradation present on the mobile satellite channel but absent on the telephone channel. First, Doppler frequency shifts due to mobile vehicle motion can be a serious source of performance degradation if not compensated for. Second, the fact that the 5-kHz mobile channel is actually a slot in a frequency-division multiple access (FDMA) system brings on the problem of interference due to energy spillover from adjacent channels. Third, the satellite channel is inherently a nonlinear one primarily due to the HPA in the transmitter. Thus, one must either employ constant envelope modulations and operate at full power or, if using a nonconstant envelope, but bandwidth-efficient modulations such as QAM, the HPA operating point must be backed off in power to produce an approximately linear channel. The most serious source of impairment that does not exist on the telephone channel is the combination of multipath fading and shadowing, i.e., for reliable performance, the system must combat short fades and recover quickly from long fades. Fading, which for mobile satellite channels can be assumed to be modelled by a Rician distribution, not only introduces an error floor into the system but also makes the problem of carrier recovery more difficult. Depending on the ratio of direct and specular (coherent component) to diffuse (noncoherent component) signal power, one might even be required to employ differentially coherent or noncoherent detection techniques, thus sacrificing the power saving associated with coherent detection. Finally,

even if the above sources of degradation were absent, the power limitation imposed by the mobile satellite channel would preclude transmission at the high data rates achievable on the telephone channel.

Also, whatever technique is decided upon must be able to be implemented and installed in the vehicle with a minimum of cost and complexity, perhaps two orders of magnitude less than that associated with a telephone channel modem.

This report shows that the combination of trellis coding and MPSK signaling with the addition of asymmetry to the signal set is a desirable modulation/coding scheme for the fading mobile satellite channel. For MPSK, introducing nonuniformity (asymmetry) into the spacing between signal points in the constellation (see Figure 1 for example) buys a further improvement in performance over that achievable with trellis coded symmetric MPSK, all this without increasing the average or peak power, or changing the bandwidth constraints imposed on the system [4,5].

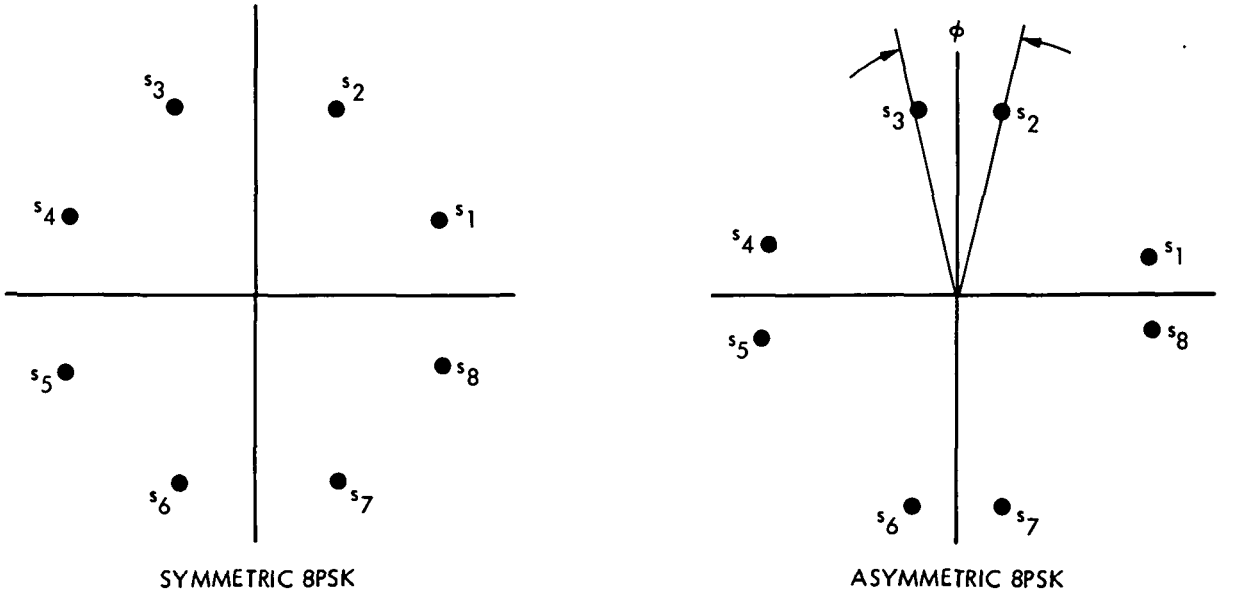

Figure 1. Symmetric and Asymmetric MPSK Signal Sets

Whereas previous contributions [2-5] have considered the performance of trellis coded modulation transmitted over an additive white Gaussian noise (AWGN) channel, the emphasis in this report is on the performance of trellis coded MPSK in the fading environment. The results will be obtained by using a combination of analysis and simulation. It will be assumed that the effect of the fading on the phase of the received signal is fully compensated for either by tracking it with some form of phase-locked loop or with pilot tone calibration techniques [6,7]. Thus, our results will reflect only the degradation due to the effect of the fading on the amplitude of the received signal. Also, we shall consider only the case where interleaving/deinterleaving is employed to further combat the fading. This allows for considerable simplification of the analysis and is of great practical interest.

SECTION II
SYSTEM MODEL

Figure 2 is a block diagram of the end-to-end system under investigation. Input bits representing data or digitally encoded speech are passed through a rate n/(n+1) trellis encoder which is normally implemented with a combination of n shift registers (the memory of the encoding operation) and appropriate mod-2 adders (XOR gates). The encoder output symbols are then block interleaved to break up burst errors caused by amplitude fades of duration greater than one symbol time. While in practice the depth of interleaving is finite and chosen in relation to the maximum fade duration anticipated, for the purpose of analysis, we shall make the usual assumption of infinite interleaving depth. This assumption provides a memoryless channel for which well-known bit error probability bounding techniques can be applied. Our simulation results will, however, reflect a finite interleaving depth. Thus, these results will be slightly pessimistic when compared with those derived from theory. The primary purpose of the analysis is to indicate through simple example the trend of the performance behavior as a function of the various system parameters leaving the actual numerical performance to be predicted by the software simulations.

Groups of n+1 interleaved symbols are mapped (with a ROM) into the MPSK signal set according to the set partitioning method [2]. The in-phase and quadrature components of the mapped signal point are digitally pulse shaped [to limit intersymbol interference (ISI)] and modulated onto quadrature carriers for transmission over the channel. If pilot tone calibration techniques [6,7] are used to recover the faded carrier at the receiver, then the pilot tone (or tones) must be added to the above data-modulated signal before transmission.

At the receiver, the faded, noise-corrupted in-phase and quadrature signal components are demodulated with the extracted pilot tone(s), q-bit quantized for soft decision decoding, and then block deinterleaved. The metric chosen for the Viterbi algorithm in the decoder depends upon whether or not channel state information (CSI) is provided [8]. As indicated in

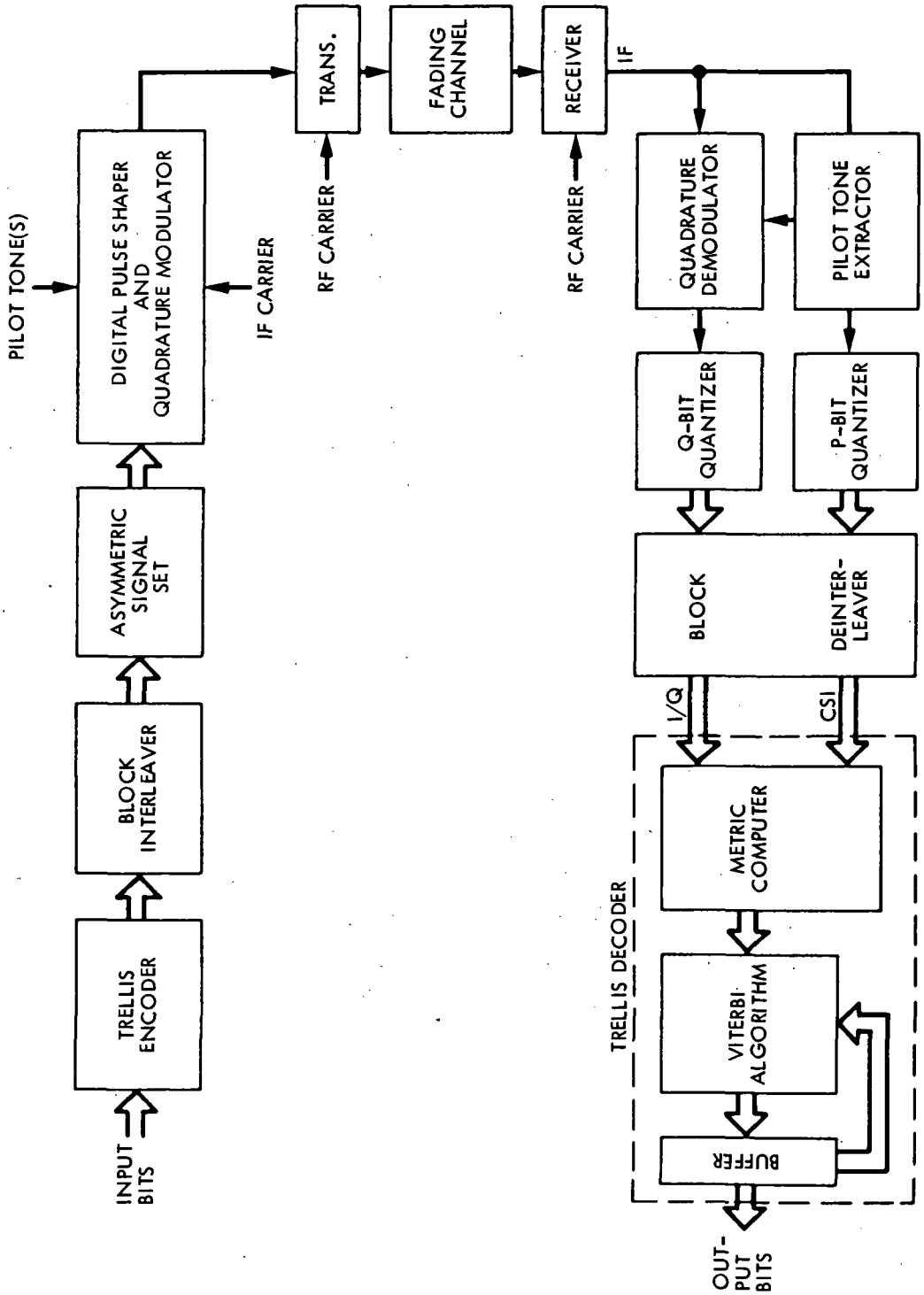

Figure 2. System Block Diagram

Figure 2, a measure of CSI can be obtained from the power in the recovered pilot tone(s). Furthermore, the number of bits of quantization, p, for this operation can be much smaller than q since the accuracy of the CSI has only a secondary effect when compared with that of the soft decisions themselves. Finally, the tentative soft decisions from the Viterbi decoder are stored in a buffer whose size is, in our application, a design parameter. In particular, for the case of speech transmission, the total coding/decoding delay must be kept below about 60 ms so as not to be objectionable to the listener. Thus, for a given input bit rate, the decoder buffer and interleaving frame sizes must be limited so as to produce at most a 60-ms delay. Again for simplicity, we shall assume an infinite buffer in the analysis, whereas the simulations will reflect a finite buffer size in accordance with the delay limitation.

SECTION III

DERIVATION OF THE PAIRWISE ERROR PROBABILITY BOUND

The basic analysis model for the system of Figure 2 is illustrated in Figure 3. The box labelled encoder is actually the combination of the trellis encoder (with binary input and output) and the mapping function of Figure 2 which, as shown in [9] can be described by a trellis encoder with binary input and M-ary output. In our notation, $M = 2^{n+1}$. Also, if the input bit rate is denoted by R_b, then the symbol rate input to the channel is R_b/n. We denote a coded symbol sequence of length N by

$$\underline{x} = (x_1, x_2, \ldots, x_N) \tag{1}$$

where the kth element of $\underline{x}$, namely x_k, represents the transmitted MPSK symbol at time k and is a nonlinear function of the state of the encoder s_k and the n information bits, $\underline{u}_k$, at its input, vis.,

$$x_k = f(s_k, \underline{u}_k) \tag{2}$$

The next state of the encoder s_{k+1} at time k+1 is a nonlinear function of the present state s_k and the n-bit input $\underline{u}_k$ which is mathematically described by

$$s_{k+1} = g(s_k, \underline{u}_k) \tag{3}$$

Corresponding to $\underline{x}$, the channel outputs the sequence

$$\underline{y} = (y_1, y_2, \ldots, y_N) \tag{4}$$

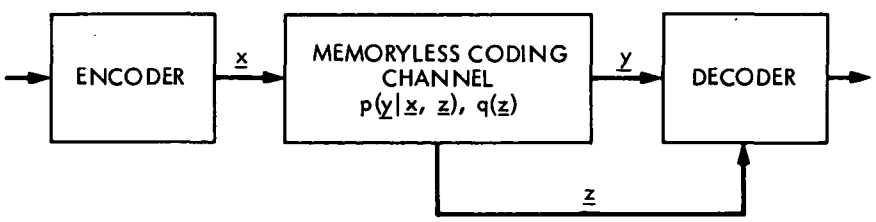

Figure 3. General Memoryless Channel

where the kth element y_k, representing the output at time k, is given by

$$y_k = \rho_k x_k + n_k \tag{5}$$

In (5), ρ_k is a normalized (unit mean-squared value) random amplitude whose probability statistics depend on the fading channel model (to be discussed later on) and n_k is a sample of a zero-mean Gaussian noise process with variance σ^2. If side information is available, the corresponding side information sequence $\underline{z}$ will be denoted by

$$\underline{z} = (z_1, z_2, \ldots, z_N) \tag{6}$$

As stated in the introduction, we shall assume adequate (theoretically infinite) interleaving and deinterleaving so that the coding channel is memoryless. Under this assumption, the ρ_k's are independent random variables (r.v.'s) and hence the channel probabilities satisfy

$$p_N(\underline{y}|\underline{x},\underline{z}) = \prod_{n=1}^{N} p(y_n|x_n,z_n) \tag{7}$$

and

$$q_n(\underline{z}) = \prod_{n=1}^{N} q(z_n) \tag{8}$$

For any coded communication system, the decoding process uses a metric of the form $m(\underline{y},\underline{x};\ \underline{z})$ if side information is available and $m(\underline{y},\underline{x})$ if it is not. Whatever metric is selected, it is desirable from the standpoint of simplifying the decoding process that it have an additive property, namely that the total metric for a sequence of symbols is the sum of the metrics for each channel input and output pair. In terms of (1), (4), and (6), this takes the form

$$m(\underline{y},\underline{x};\ \underline{z}) = \sum_{n=1}^{N} m(y_n,x_n;\ z_n) \tag{9}$$

The maximum-likelihood metric

$$m(\underline{y},\underline{x};\ \underline{z}) = \ell n\ p_N(\underline{y}|\underline{x},\underline{z}) \tag{10a}$$

when side information is available or

$$m(\underline{y},\underline{x}) = \ell n\ p_N(\underline{y}|\underline{x}) \tag{10b}$$

when no side information is available satisfies the requirement in (9). This is easily seen by substituting (7) in (10) and recalling that the logarithm of a product equals the sum of the logarithms. Thus, we shall use this metric in what follows. Also for simplicity, we shall use only the notation of (10a) keeping in mind that the case where no side information is available is a special case where the metric $m(\underline{y},\underline{x};\ \underline{z})$ does not depend on $\underline{z}$.

To find an upper bound on the average bit error probability performance of the Viterbi decoder, we must first find the pairwise error probability $P(\underline{x} \to \hat{\underline{x}})$ which represents the probability of choosing the coded sequence $\hat{\underline{x}} = (\hat{x}_1, \hat{x}_2, \ldots, \hat{x}_N)$ instead of $\underline{x} = (x_1, x_2, \ldots, x_N)$. Since the decoder incorrectly decides $\hat{\underline{x}}$ is the transmitted sequence when

$$m(\underline{y},\hat{\underline{x}};\ \underline{z}) \geq m(\underline{y},\underline{x};\ \underline{z}) \tag{11a}$$

or, equivalently

$$\sum_{n=1}^{N} m(y_n,\hat{x}_n;\ z_n) \geq \sum_{n=1}^{N} m(y_n,x_n;\ z_n), \tag{11b}$$

the pairwise probability $P(\underline{x} \to \hat{\underline{x}})$ is given by

$$P(\underline{x} \to \hat{\underline{x}}) = \Pr\left\{\sum_{n=1}^{N} m(y_n,\hat{x}_n;\ z_n) \geq \sum_{n=1}^{N} m(y_n,x_n;\ z_n)\,|\underline{x}\right\} \tag{12}$$

Applying the Chernoff bound, (12) becomes [10]

$$P(\underline{x} \to \hat{\underline{x}}) \leq \prod_{n\varepsilon\eta} E\{\exp\ (\lambda[m(y_n,\hat{x}_n;\ z_n) - m(y_n,x_n;\ z_n)])|\underline{x}\} \tag{13}$$

where "E" is the statistical expectation operation, λ is the Chernoff parameter to be optimized, and η is the set of all n such that $x_n \neq \hat{x}_n$. To simplify (13) further, we must specify whether or not side information is available.

A. IDEAL CHANNEL STATE INFORMATION

The assumption of ideal channel state information is tantamount to assuming that the side information r.v. z_n is equal to the fading amplitude ρ_n. Thus, since n_n is Gaussian distributed and in general, x_n and y_n are complex quantities, then using (5) and (10a) gives

$$m(y_n,x_n;\ z_n) = -\ |y_n - \rho_n x_n|^2 \tag{14}$$

where for simplicity we shall ignore the $1/2\sigma^2$ factor since it would later be absorbed in the Chernoff bound parameter λ anyway. Substituting (14) into (13) and conditioning on $\underline{\rho}$ we get

$$P(\underline{x} \to \hat{\underline{x}}|\underline{\rho}) \leq \prod_{n\varepsilon\eta} \exp\ [-\lambda\rho_n^2|x_n - \hat{x}_n|^2]\ E\{\exp\ [-2\lambda\rho_n Re\{n_n(x_n - \hat{x}_n)^*\}]\} \tag{15}$$

Representing the complex noise r.v. n_n in terms of its real and imaginary parts where $Re\{n_n\}$ and $Im\{n_n\}$ are uncorrelated zero-mean Gaussian r.v.'s, each with variance $\sigma_N^2 = \sigma^2/2$, it can be shown that

$$E\{\exp\ [-2\lambda\rho_n Re\{n_n(x_n - \hat{x}_n)^*\}]\} = \exp\ [2\lambda^2\rho_n^2\sigma_N^2|x_n - \hat{x}_n|^2] \tag{16}$$

Substituting (16) into (15) gives after some simplification

$$P(\underline{x} \to \hat{\underline{x}}|\underline{\rho}) \leq \prod_{n\varepsilon\eta} \exp\ [-\lambda\rho_n^2|x_n - \hat{x}_n|^2(1 - 2\lambda\sigma_N^2)] \tag{17}$$

Since σ_N^2 is independent of n, optimizing (17) over the Chernoff bound parameter λ yields

$$\lambda_{opt} = \frac{1}{4\sigma_N^2} \tag{18}$$

which when substituted in (17) produces the desired result, namely,

$$P(\underline{x} \to \hat{\underline{x}}|\underline{\rho}) \leq \prod_{n\epsilon\eta} D^{\rho_n^2|x_n - \hat{x}_n|^2}; \quad D = \exp(-1/8\sigma_N^2) \tag{19}$$

Finally, (19) can be rewritten as

$$P(\underline{x} \to \hat{\underline{x}}|\underline{\rho}) \leq D^{d^2(\underline{x},\hat{\underline{x}})} \tag{20}$$

where

$$d^2(\underline{x},\hat{\underline{x}}) \triangleq \sum_{n\epsilon\eta} \rho_n^2|x_n - \hat{x}_n|^2 \tag{21}$$

represents the square of the weighted Euclidean distance between the two symbol sequences $\underline{x}$ and $\hat{\underline{x}}$.

Finally, the pairwise error probability upperbound is obtained by averaging (20) over the probability density function (p.d.f.) of $\underline{\rho}$.

B. NO CHANNEL STATE INFORMATION

When no channel state information is available, then the metric of (10b) becomes

$$m(y_n,x_n) = -|y_n - x_n|^2 \tag{22}$$

Substituting (5) into (22), then, analogous to (15), we now get

$$P(\underline{x} \to \hat{\underline{x}}|\underline{\rho}) \leq \prod_{n\varepsilon\eta} \exp\left[-\lambda|x_n - \hat{x}_n|^2 - 2\lambda(\rho_n - 1)\,\mathrm{Re}\{x_n(x_n - \hat{x}_n)^*\}\right]$$

$$\times\, E\{\exp\left[-2\lambda\rho_n\,\mathrm{Re}\{n_n(x_n - \hat{x}_n)^*\}\right]\} \tag{23}$$

Again using (16), Eq. (23) simplifies to

$$P(\underline{x} \to \hat{\underline{x}}|\underline{\rho}) \leq \prod_{n\varepsilon\eta} \exp\left[-\lambda|x_n - \hat{x}_n|^2(1 - 2\lambda\sigma_N^2)\right.$$

$$\left. - 2\lambda(\rho_n - 1)\,\mathrm{Re}\{x_n(x_n - \hat{x}_n)^*\}\right] \tag{24}$$

For constant envelope signal sets such as MPSK where $|x|^2 = |\hat{x}|^2$, (24) can be further simplified by noting that

$$|x - \hat{x}|^2 = 2\mathrm{Re}\{x(x - \hat{x})^*\} \tag{25}$$

Thus, substituting (25) into (24) and renormalizing the Chernoff parameter (i.e., replace λ by $2\lambda\sigma_N^2$), we get the desired result analogous to (17), namely,

$$P(\underline{x} \to \hat{\underline{x}}|\underline{\rho},\lambda) \leq D^{c^2(\underline{x},\hat{\underline{x}}|\underline{\rho},\lambda)} \tag{26}$$

where D is again given by (19) and

$$c^2(\underline{x},\hat{\underline{x}}|\underline{\rho},\lambda) = \sum_{n\varepsilon\eta} 4\lambda(\rho_n - \lambda)|x_n - \hat{x}_n|^2$$

$$= 4\lambda \sum_{n\varepsilon\eta} \rho_n|x_n - \hat{x}_n|^2 - 4\lambda^2 d^2(\underline{x},\hat{\underline{x}}) \tag{27}$$

Note that unlike (17), Eq. (26) cannot be optimized over λ to yield a constant value for this parameter. Thus, in this case, we must first average over the fading distribution.

SECTION IV

DERIVATION OF THE BIT ERROR PROBABILITY BOUND

To derive the upper bound on bit error probability from the pairwise error probability bound, we follow the transfer function approach taken in [5]. In particular, we first find the unconditioned pairwise error probability by averaging (20) or (26) over the p.d.f. of ρ. (This averaging will be denoted by an overbar.) When this is done, the pairwise error probability can be expressed in the form*

$$P(\underline{x} \to \hat{\underline{x}}) = \overline{D^{\Delta}} \tag{28}$$

where for the ideal channel state information case

$$\Delta = \sum_{n \in \eta} \rho_n^2 |x_n - \hat{x}_n|^2 \tag{29a}$$

and for the no channel state information case

$$\Delta = \sum_{n \in \eta} 4\lambda(\rho_n - \lambda) \, |x_n - \hat{x}_n|^2 \tag{29b}$$

In dealing with upper bounds of this type, it is convenient to work with a pair-state transition diagram [11] where the pair-state S_k and pair-information symbol U_k are defined as

$$\begin{aligned} S_k &\triangleq (s_k, \hat{s}_k) \\ U_k &\triangleq (u_k, \hat{u}_k) \end{aligned} \tag{30}$$

*For uniformity of notation, we shall drop the dependence of the pairwise error probabilty on λ for the no channel state information case.

where $\hat{s}_k$ and $\hat{u}_k$ are the estimates for the state of the decoder and the information symbol, respectively. We are in a correct pair-state when $\hat{s}_k = s_k$ and in an incorrect pair-state when $\hat{s}_k \neq s_k$. Substituting (2) into (29), we can write the latter as

$$\Delta = \sum_{n \in \eta} \delta^2(S_n, U_n) \tag{31}$$

where

$$\delta^2(S_n, U_n) = \rho_n^2 |f(s_n, u_n) - f(\hat{s}_n, \hat{u}_n)|^2 \tag{32a}$$

or

$$\delta^2(S_n, U_n) = 4\lambda(\rho_n - \lambda)|f(s_n, u_n) - f(\hat{s}_n, \hat{u}_n)|^2 \tag{32b}$$

When no fading is present, (28) is given by [5]

$$P(\underline{x} \to \hat{\underline{x}}) = D^{\Delta} \tag{33}$$

where Δ is still of the form in (31) with, however,

$$\delta^2(S_n, U_n) = |f(s_n, u_n) - f(\hat{s}_n, \hat{u}_n)|^2 \tag{34}$$

In terms of the above definitions, it can be shown by analogy with the results in [5] that the average bit error probability P_b is upper bounded by

$$P_b \leq \frac{1}{n} \frac{d}{dI} \bar{T}(D, I)\Big|_{I=1} \tag{35}$$

where $\bar{T}(D,I)$ is the transfer function of the pair-state transition diagram whose branch label gains are modified from those for the no fading case as follows. In the absence of fading each branch label gain has a factor $D^{\delta^2(S_n,U_n)}$ where $\delta^2(S_n,U_n)$ is given by (34). For the fading case, we simply replace $D^{\delta^2(S_n,U_n)}$ by $\overline{D^{\delta^2(S_n,U_n)}}$ where again the overbar denotes

averaging over the p.d.f. of ρ and $\delta^2(S_n,U_n)$ is given by (32a) or (32b) as appropriate depending on the availability of channel state information.

Finally, for the case of no channel state information, we must minimize the upper bound of (35) over the Chernoff parameter to obtain the tightest upper bound. Recall that for the ideal channel state information case, we were able to perform this optimization at the pairwise error probability level.

SECTION V

CHARACTERIZATION OF THE FADING CHANNEL

For mobile satellite communication, multipath fading produces a received signal with an amplitude* which can be modelled by Rician statistics with parameter K representing the ratio of the power in the direct (line-of-sight) and specular component to that in the diffuse component. If shadowing is severe, then a Rayleigh statistical model becomes appropriate which can be looked upon as the limiting case of a Rician channel when K approaches zero. Of course, the case of no fading corresponds to a Rician channel with K approaching infinity.

Mathematically speaking, the above statements correspond to a p.d.f. for the fading r.v. given by

$$p(\rho) = \begin{cases} 2\rho(1 + K) \exp\left[-K - \rho^2(1 + K)\right] I_0\left(2\rho \sqrt{K(1 + K)}\right); & \rho \geq 0 \\ 0 \ ; \quad \text{otherwise} \end{cases} \tag{36}$$

where $I_0(x)$ is the zero-order modified Bessel function of the first kind.

*We assume that the phase distortion produced by the fading is fully compensated for either by tracking it with some form of phase-locked loop or with pilot tone calibration techniques [6,7].

SECTION VI
AN EXAMPLE

Consider the case of rate 1/2 trellis coded asymmetric QPSK using a 2-state trellis. The appropriate set partitioning is illustrated in Figure 4, the trellis diagram in Figure 5, and the pair-state transition diagram in Figure 6. The performance of this system in the absence of fading was treated in [5] with the following results:

$$T(D,I) = \frac{4ac}{1 - 2b} \; ; \quad a = \frac{I}{2} D^4 \; ; \quad b = \frac{I}{2} D^{\frac{4}{1+\alpha}} \; ; \quad c = \frac{1}{2} D^{\frac{4\alpha}{1+\alpha}} \tag{37a}$$

or

$$T(D,I) = \frac{ID^{\frac{4(1+2\alpha)}{1+\alpha}}}{1 - ID^{\frac{4}{1+\alpha}}} \tag{37b}$$

where D as defined in (19) becomes [5]

$$D = \exp\left(-\frac{E_b}{4N_0}\right) \; ; \quad \frac{E_b}{N_0} = \text{system bit energy-to-noise spectral density ratio} \tag{38}$$

and α is the ratio of powers between the I and Q channels which is related to the angle ϕ that defines the asymmetry (see Figure 4) by

$$\alpha = \tan^2 \frac{\phi}{2} \tag{39}$$

Substituting (37) into (35) gives

$$P_b \leq \frac{D^{\frac{4(1+2\alpha)}{1+\alpha}}}{\left(1-D^{\frac{4}{1+\alpha}}\right)^2} \tag{40}$$

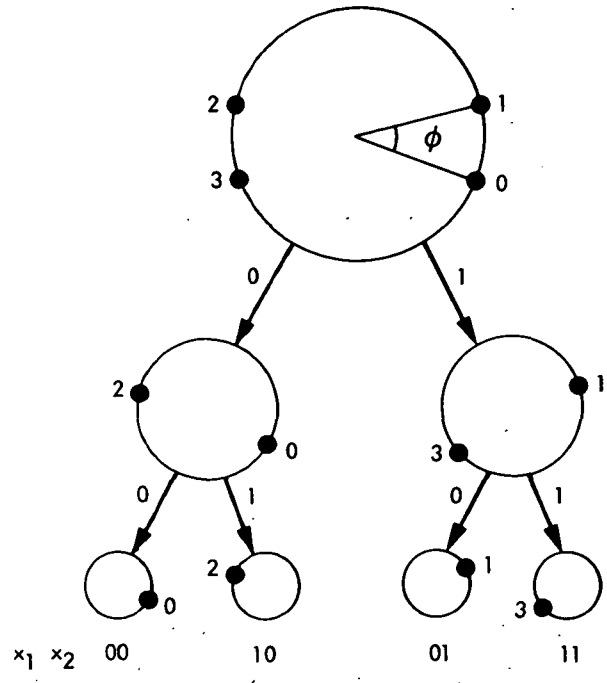

Figure 4. Set Partitioning of Asymmetric 4-PSK

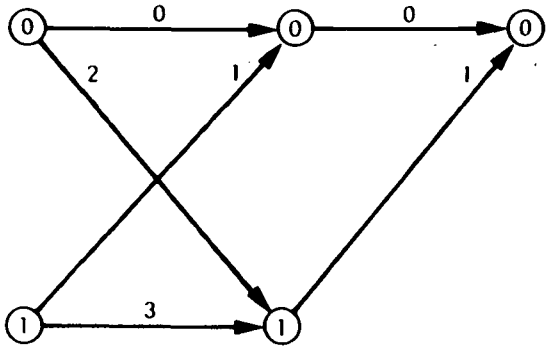

Figure 5. Trellis Diagram and MPSK Signal Assignment for 4-PSK

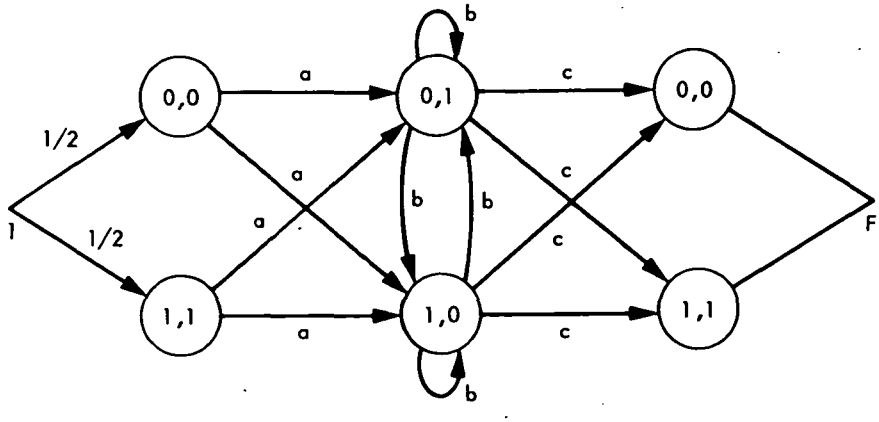

Figure 6. Pair-State Transition Diagram for Figure 5

Optimizing (40) over the asymmetry produces

$$\alpha = -\frac{4\ \ln D}{\ln 3} - 1 = \frac{E_b/N_0}{\ln 3} - 1 \tag{41}$$

which when substituted into (40) gives the desired upper bound

$$P_b \leq \frac{27}{4} \exp\ (-2E_b/N_0) \tag{42}$$

A. IDEAL CHANNEL STATE INFORMATION

Recalling (29a), we see that the transfer function $\bar{T}(D,I)$ of the pair-state transition diagram for the case of ideal channel state information is obtained merely by replacing D^{β} by $D\rho^{2\beta}$ in the branch label gains of (37a) where $\beta = 4$, $4/(1+\alpha)$, or $4\alpha/(1+\alpha)$ as appropriate. For the Rician p.d.f. of (36), $D\rho^{2\beta}$ evaluates to*

$$\overline{D\rho^{2\beta}} = \left(\frac{1+K}{1+K+\beta\gamma}\right) D^{\frac{\beta K}{1+K+\beta\gamma}} ; \quad \gamma = \frac{\overline{E_b}}{4N_0} \tag{43a}$$

which for the Rayleigh special case (K = 0) becomes

$$\overline{D\rho^{2\beta}} = \frac{1}{1+\beta\gamma} \tag{43b}$$

Evaluating T(D,I) of (37a) using (43) and performing the differentiation required in (35) gives the upper bound on P_b as

$$P_b \leq \frac{\xi_1\xi_3\, D^{\zeta_1+\zeta_3}}{\left(1 - \xi_2\, D^{\zeta_2}\right)^2} \tag{44}$$

---

*Note that $\overline{E_b}$ represents the total average received power (direct plus specular plus diffuse) in the data bandwidth. In the general case of an n/(n+1) code rate, $\overline{E_b}$ in the definition of λ would be replaced by $n\overline{E_b}$.

where

$$\zeta_i = \frac{\beta_i K}{1 + K + \beta_i \gamma} \; ; \quad \xi_i = \frac{1 + K}{1 + K + \beta_i \gamma} \; ; \quad i = 1, 2, 3$$

$$\beta_1 = 4 \; ; \quad \beta_2 = \frac{4}{1 + \alpha} \; ; \quad \beta_3 = \frac{4\alpha}{1 + \alpha} \tag{45}$$

To obtain the best performance in the presence of fading, one should optimize (44) over the asymmetry parameter α. Before doing this, however, we shall first examine the behavior of (44) for the symmetric case, i.e., $\alpha = 1$, and the optimum asymmetry in the absence of fading as given by (41).

Substituting $\alpha = 1$ in (45), the parameters ξ_i and ζ_i simplify to

$$\zeta_1 = \frac{4K}{1 + K + 4\gamma} \quad ; \quad \xi_1 = \frac{1 + K}{1 + K + 4\gamma}$$

$$\zeta_2 = \zeta_3 = \frac{2K}{1 + K + 2\gamma} \quad ; \quad \xi_2 = \frac{1 + K}{1 + K + 2\gamma} \tag{46}$$

The curve labelled "symmetric" on Figure 7 is a plot of the upper bound of (44) combined with (46) as a function of the average bit energy-to-noise ratio $\overline{E_b}/N_0$ with a Rician parameter K = 10 (typical of the mobile satellite channel).

When the value of α in (41) is substituted in (45), after some simplification (44) and (45) can be written as

$$P_b \leq \frac{\xi_1' \xi_3' \exp\left[-(\zeta_1' + \zeta_2')\right]}{\left(1 - \xi_2' \exp\left(-\zeta_2'\right)\right)^2} \tag{47}$$

and

$$\zeta_i' = \frac{\beta_i' K}{1 + K + \beta_i'} \; ; \quad \xi_i' = \frac{1 + K}{1 + K + \beta_i'} \; ; \quad i = 1, 2, 3$$

$$\beta_1' = \frac{E_b}{N_0} \; ; \quad \beta_2' = \ln 3 \; ; \quad \beta_3' = \frac{E_b}{N_0} - \ln 3 \tag{48}$$

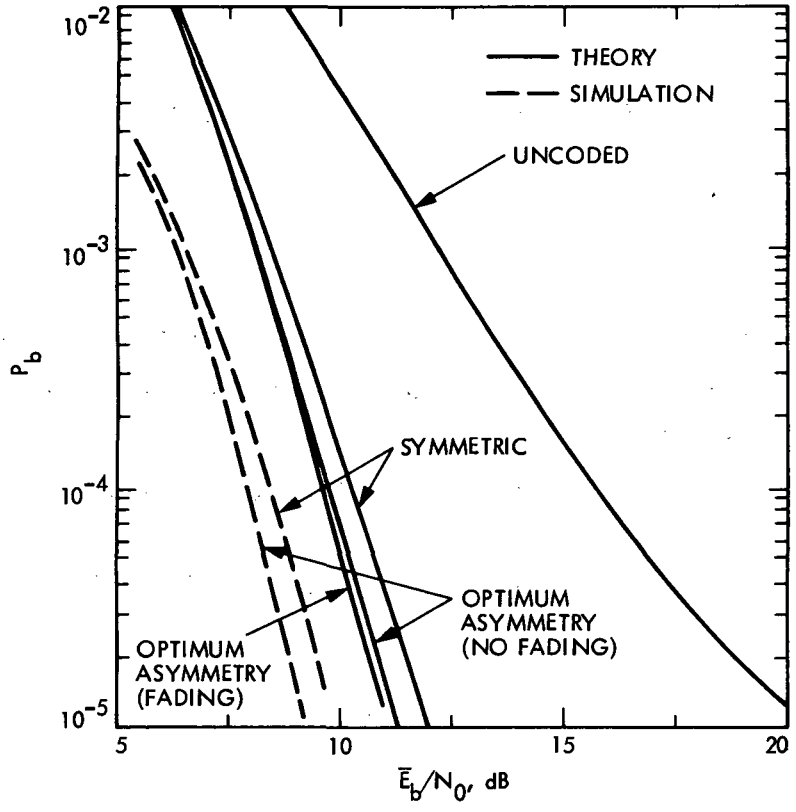

Figure 7. Bit Error Probability Performance vs $\bar{E}_b/N_0$ for Rate 1/2 Trellis Coded QPSK in the Presence of Rician Fading; 2 States, K = 10; Ideal Channel State Information

The behavior of (47) combined with (48) is also illustrated Figure 7 by the curve labelled "optimum asymmetry (no fading)."

For the Rayleigh case, the above results simplify even further. In particular, for the symmetric signal QPSK constellation, we get

$$P_b \leq \left(\frac{1 + \bar{E}_b/2N_0}{\bar{E}_b/2N_0}\right)^2 \left(\frac{1}{1 + \bar{E}_b/N_0}\right)\left(\frac{1}{1 + \bar{E}_b/2N_0}\right) \tag{49}$$

whereas for the optimum asymmetry in the absence of fading,

$$P_b \leq \left(\frac{1 + \ell n3}{\ell n3}\right)\left(\frac{1}{1 + \bar{E}_b/N_0}\right)\left(\frac{1}{1 + \bar{E}_b/N_0 - \ell n3}\right) \tag{50}$$

These results are illustrated in Figure 8. Note that here the curve labelled "optimum asymmetry (no fading)" gives worse performance than that of the symmetric case. Thus, at least here, we clearly see the need for performing the asymmetry optimization in the presence of the fading.

To determine the optimum value of α for the Rician case, we need to differentiate (44) with respect to α and equate the result to zero. This leads to a transcendental equation which must be solved numerically. Rather than doing that, it is more expedient to directly minimize (44) with respect to α using numerical techniques. When this is done, we obtain the optimum bit error probability bound labelled "optimum asymmetry (fading)" in Figure 7. For K = 10, this curve lies quite close to the "optimum asymmetry (no fading)" curve. However, as we can already deduce from Figure 8, this statement is not true for small values of K, in particular the Rayleigh

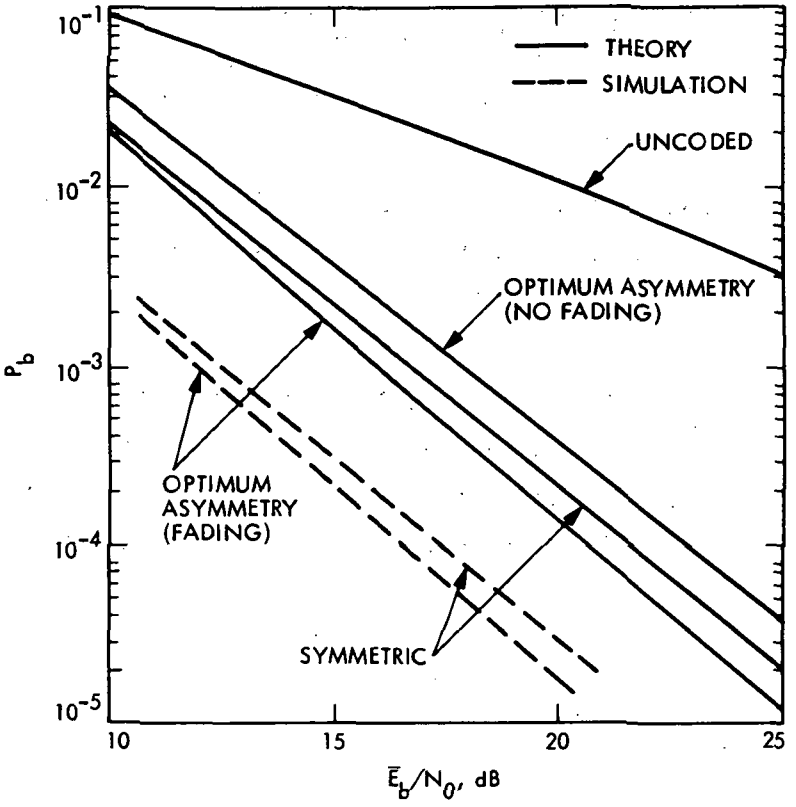

Figure 8. Bit Error Probability Performance vs $\bar{E}_b/N_0$ for Rate 1/2 Trellis Coded QPSK in the Presence of Rayleigh Fading; 2 States; Ideal Channel State Information

channel with K = 0. To exhibit the sensitivity of the optimum asymmetry condition to K, Figure 9 illustrates the optimum value of α as a function of $\bar{E}_b/N_0$ with K as a parameter.

For the Rayleigh case, we can indeed determine the optimum asymmetry condition in closed form. In particular, differentiating (44) with K = 0 in (45) and equating the result to zero has the solution

$$\alpha = \frac{-4 + \bar{E}_b/N_0 \left(\sqrt{17 + 8\bar{E}_b/N_0} - 1\right)}{4(1 + \bar{E}_b/N_0)} \tag{51}$$

which when substituted back in (44) gives

$$P_b \leq \frac{(3 + \sqrt{17 + 8\bar{E}_b/N_0})\,[4(\bar{E}_b/N_0)^2 + (\bar{E}_b/N_0)^2(7 + \sqrt{17 + 8\bar{E}_b/N_0})]^2}{16(\sqrt{17 + 8\bar{E}_b/N_0} - 1)(\bar{E}_b/N_0)^2(1 + \bar{E}_b/N_0)^4} \tag{52}$$

This result is illustrated by the curve labelled "optimum asymmetry (fading)" in Figure 8 and is clearly superior to that corresponding to the symmetric signal constellation.

Finally, for purpose of comparison, the corresponding upper bound on the performance of uncoded BPSK (same bandwidth as rate 1/2 trellis coded QPSK) in the presence of Rician and Rayleigh fading is also illustrated in Figures 7 and 8. The analytical results for these curves are well known and are given by

$$P_b \leq \frac{1 + K}{1 + K + \bar{E}_b/N_0} \exp\left(-\frac{K\bar{E}_b/N_0}{1 + K + \bar{E}_b/N_0}\right) \tag{53}$$

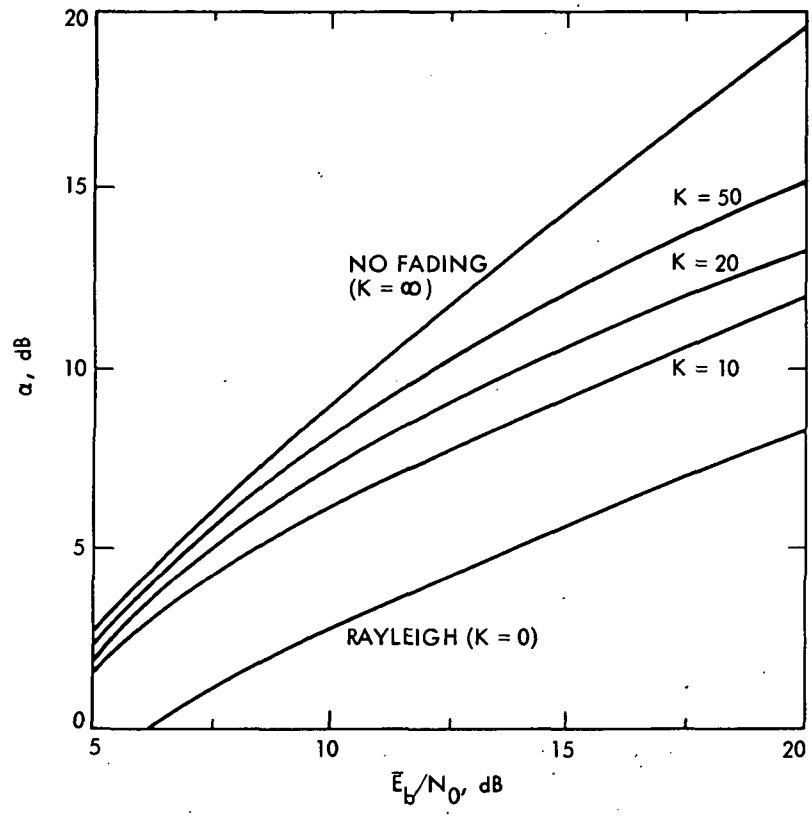

Figure 9. Optimum Asymmetry Parameter vs $\bar{E}_b/N_0$ for Rate 1/2 Trellis Coded QPSK in the Presence of Rician Fading

for the Rician channel and

$$P_b \leq \frac{1}{1 + \bar{E}_b/N_0} \tag{54}$$

for the Rayleigh channel.

Depending on the shape of the bit error probability vs $\bar{E}_b/N_0$ curve, one can often deduce some important practical conclusions by examining the asymptotic behavior of the curve. Since for the Rayleigh case (Figure 8), the error probability performance curves are essentially linear over a wide range of practical SNRs, one can approximately apply the asymptotic (large $\bar{E}_b/N_0$) result over this domain. In particular, for large $\bar{E}_b/N_0$, (49), (50), (52), and (54), respectively, become

$$P_b \lesssim \frac{1}{(\sqrt{2}\bar{E}_b/N_0)^2} \qquad \text{(symmetric)} \qquad (49')$$

$$P_b \lesssim \frac{1}{\left[\left(\frac{\ell n\ 3}{1 + \ell n\ 3}\right)\frac{\bar{E}_b}{N_0}\right]^2} \qquad \text{(optimum asymmetry - no fading)} \qquad (50')$$

$$P_b \lesssim \frac{1}{(\bar{E}_b/N_0)^2} \qquad \text{(optimum asymmetry - fading)} \qquad (52')$$

and

$$P_b \lesssim \frac{1}{\bar{E}_b/N_0} \qquad \text{(uncoded)} \qquad (54')$$

Thus, for example, comparing (49') with (54'), we see that the effect of coding is to change the rate of descent of the error probability vs. $\bar{E}_b/N_0$ performance from an inverse linear to an inverse square law behavior. If the QPSK constellation is now designed according to the optimum asymmetry for no fading, the performance is worse than that of the symmetric constellation by a factor of $(1 + \ell n\ 3)/(\sqrt{2}\ \ell n\ 3)$ or 1.3 dB. On the other hand, if the constellation is designed with the optimum asymmetry determined in the presence of fading, then, relative to the symmetric design, the performance is improved by a factor of $\sqrt{2}$ or 1.5 dB. From Figure 8, we see that these asymptotic results are almost achieved at an error rate of 10^{-5}.

B. NO CHANNEL STATE INFORMATION

Recalling (29b), we see that the transfer function $\bar{T}(D,I)$ of the pair-state transition diagram for the case of no channel state information is obtained by replacing D^{β}, this time by $\overline{D^{4\lambda(\rho-\lambda)\beta}} = D^{-4\lambda^2\beta}\overline{D^{4\lambda\beta\rho}}$ in the branch label gains of (37a) where again $\beta = 4$, $4/(1 + \alpha)$, or $4\alpha/(1 + \alpha)$ as appropriate. Unfortunately, for the Rician distribution, the factor $\overline{D^{4\lambda\beta\rho}}$ cannot

be evaluated in closed form. It can, however, be expressed as a single integral with finite limits as follows:

$$\overline{D^{4\lambda\beta\rho}} = e^{-K}\left[1 - \frac{1}{\sqrt{\pi}}\int_0^{\pi} \eta(\theta)\, \exp\,[\eta^2(\theta)]\, \operatorname{erfc}\, \eta(\theta)\, d\theta\right]$$

$$\eta(\theta) = \frac{\lambda\beta(\bar{E}_b/2N_0)}{\sqrt{1+K}} - \sqrt{K}\cos\theta \tag{55}$$

This integral is easily evaluated using Gauss-Chebyshev techniques, i.e.,

$$\int_0^{\pi} \eta(\theta)\, \exp\,[\eta^2(\theta)]\, \operatorname{erfc}\, \eta(\theta)\, d\theta \tilde{=} \frac{\pi}{N}\sum_{k=1}^{N} \eta(\theta_k)\, \exp\,[\eta^2(\theta_k)]\, \operatorname{erfc}\, \eta(\theta_k) \tag{56}$$

where $\theta_k \triangleq (2k-1)\pi/2N$.

For the Rayleigh case, we can obtain a closed form result for this factor since, for $K = 0$, $\eta(\theta)$ becomes independent of θ. Thus,

$$\overline{D^{4\lambda\beta\rho}} = 1 - \sqrt{\pi}\lambda\beta\left(\frac{\bar{E}_b}{2N_0}\right)\exp\left[\left(\lambda\beta\frac{\bar{E}_b}{2N_0}\right)^2\right]\operatorname{erfc}\left(\lambda\beta\,\frac{\bar{E}_b}{2N_0}\right) \tag{57}$$

Evaluating $\overline{T}(D,I)$ of (37a) using (55) and performing the differentiation required in (35) gives the upper bound

$$P_b \leq \min_{\lambda\geq 0}\ \min_{\alpha}\ \frac{\xi_1\xi_3\, D^{-16\lambda^2(1+2\alpha)/(1+\alpha)}}{\left(1 - \xi_2\, D^{-16\lambda^2/(1+\alpha)}\right)^2} \tag{58}$$

where

$$\xi_i \triangleq e^{-K}\left[1 - \frac{1}{\sqrt{\pi}} \int_0^{\pi} \eta_i(\theta) \exp\left(\eta_i^2(\theta)\right) \operatorname{erfc} \eta_i(\theta)\, d\theta\right]$$

$$\eta_i(\theta) \triangleq \frac{\lambda \beta_i (\bar{E}_b/2N_0)}{\sqrt{1+K}} - \sqrt{K}\cos\theta \tag{59}$$

and β_i; $i = 1, 2, 3$ are defined in (45). For the Rayleigh case one merely replaces ξ_i and $\eta_i(\theta)$ of (59) by

$$\xi_i \triangleq 1 - \sqrt{\pi}\,\eta_i \exp\left(\eta_i^2\right) \operatorname{erfc} \eta_i$$

$$\eta_i \triangleq \lambda \beta_i (\bar{E}_b/2N_0) \tag{60}$$

and performs the same minimizations required in (58).

Figures 10 and 11 illustrate the analogous results to Figures 7 and 8 for the case where no channel state information is available.* Clearly, the lack of channel state information produces a noticeable degradation in system performance. To quantitatively assess this additional degradation (at least for the Rayleigh channel), we now derive asymptotic results analogous to (49'), (50'), and (52') for the no channel state information case. In particular, we use the asymptotic (large argument) expansion for erfc x, i.e.,

$$\operatorname{erfc} x \tilde{=} \frac{\exp\left(-x^2\right)}{\sqrt{\pi}\, x}\left[1 - \frac{1}{2}\, x^{-2}\right] \tag{61}$$

in which case (57) simplifies to

$$\overline{P_D^{4\lambda\beta\rho}} \tilde{=} \frac{1}{2[\lambda\beta(\bar{E}_b/2N_0)]^2} \tag{62}$$

*For simplicity of presentation, we have chosen not to illustrate the results for the values of optimum asymmetry determined from the no fading analysis since we have already made the point that asymmetry should be optimized in the fading environment.

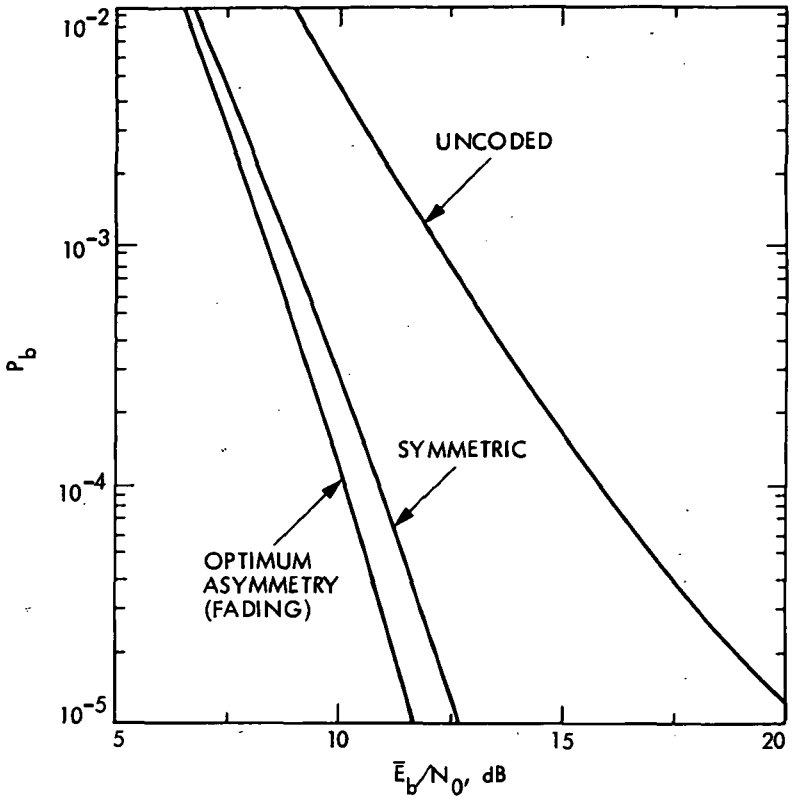

Figure 10. Bit Error Probability Performance vs $\bar{E}_b/N_0$ for Rate 1/2 Trellis Coded QPSK in the Presence of Rician Fading; 2 States, K = 10; No Channel State Information

Using the appropriate values of ß in (62), the branch gains of Figure 6 become

$$a = \frac{I}{4(2\lambda\bar{E}_b/N_0)^2} \exp\left(4\lambda^2\bar{E}_b/N_0\right)$$

$$b = \frac{I}{4\left(\frac{2\lambda\bar{E}_b/N_0}{1+\alpha}\right)^2} \exp\left(\frac{4\lambda^2\bar{E}_b/N_0}{1+\alpha}\right) \qquad (63)$$

$$c = \frac{1}{4\left(\frac{2\alpha\lambda\bar{E}_b/N_0}{1+\alpha}\right)^2} \exp\left(\frac{4\alpha\lambda^2\bar{E}_b/N_0}{1+\alpha}\right)$$

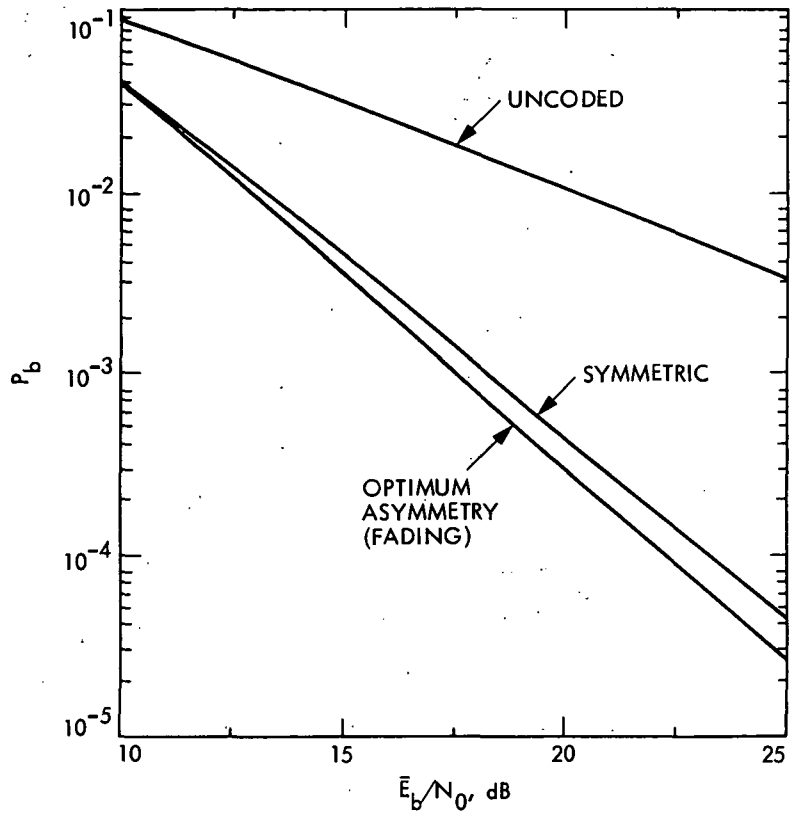

Figure 11. Bit Error Probability Performance vs $\bar{E}_b/N_0$ for Rate 1/2 Trellis Coded QPSK in the Presence of Rayleigh Fading; 2 States; No Channel State Information

Substituting (63) into the transfer function of (37a) and performing the differentiation required in (35) gives the approximate upper bound on P_b (valid for large E_b/N_0)

$$P_b \lesssim \min_{\lambda} \frac{\exp\left(\frac{4(1+2\alpha)}{1+\alpha}\lambda^2\bar{E}_b/N_0\right)}{4(2\gamma\bar{E}_b/N_0)^4\left(\frac{\alpha}{1+\alpha}\right)^2} \times \left\{1 - \frac{1}{2\left(\frac{2\gamma\bar{E}_b/N_0}{1+\alpha}\right)^2}\exp\left(\frac{4}{1+\alpha}\gamma^2\bar{E}_b/N_0\right)\right\}^{-2} \tag{64}$$

Performing the minimization over λ required in (64) (actually we minimize only the numerator since the denominator has little effect on this operation) gives

$$\lambda_{opt} = \frac{1}{2\left(\frac{1 + 2\alpha}{1 + \alpha}\right)(\bar{E}_b/N_0)} \tag{65}$$

which when substituted in (64) yields

$$P_b \lesssim \left(\frac{1 + 2\alpha}{\alpha}\right)^2 \frac{e^2}{16(\bar{E}_b/N_0)^2} \tag{66}$$

Finally, the desired asymptotic results are

$$P_b \lesssim \frac{9e^2}{16(\bar{E}_b/N_0)^2} \qquad \text{(symmetric)}$$

$$P_b \lesssim \left(\frac{2\bar{E}_b/N_0 - \ell n 3}{\bar{E}_b/N_0 - \ell n 3}\right)^2 \frac{e^2}{16(\bar{E}_b/N_0)^2} \qquad \text{(optimum asymmetry - no fading)} \tag{67}$$

$$P_b \lesssim \frac{e^2}{4(\bar{E}_b/N_0)^2} \qquad \text{(optimum asymmetry - fading)}$$

SECTION VII
SIMULATION RESULTS

In this section, we describe and present the results of a software simulation of the system block diagram of Figure 2. For the application at hand, the development of a simulation has a manyfold purpose. First, it can be used to "verify" the theoretical results obtained in the previous section keeping in mind that the simulation is indicative of the exact system performance whereas the theoretical bit error rate expressions are upper bounds. Second, when the number of states in the trellis diagram becomes large (e.g., 16), determining the state transition diagram and its associated transfer function is a tedious task; in such cases, simulation is the more expedient approach. Finally, system degradation due to the finite size of interleaving and decoder buffer imposed by the practical constraint on the allowable total delay is analytically intractable, particularly when coupled with that caused by the "noisy" carrier demodulation reference produced by the pilot tone extractor. Hence, to predict true system performance corresponding to the real world environment, one must again turn to simulation. In the next paragraph, we expand upon the last of these issues.

The block interleaver of Figure 2 can be regarded as a buffer with d rows which represent the depth of interleaving and s columns which represent the span of interleaving. Thus, the size of the interleaver (in symbols) is d x s. Data is written into the buffer in successive rows and read out of the buffer (the order in which it is transmitted over the channel) in columns. At the receiver, the block deinterleaver performs the reverse operation, i.e., the received soft quantized symbols are written into the buffer in successive columns and read out in rows. In practice, the interleaving depth should be chosen on the order of the maximum fade depth anticipated which, for the fading mobile satellite channel under investigation, depends on the doppler frequency or, equivalently, the vehicle speed. The smaller the doppler frequency, the longer the fade duration and vice versa. The interleaving span should be chosen on the order of the decoder buffer size. When this is done, the performance degradation (relative to that for the analytically tractable

assumption of infinite interleaving depth and buffer size) will be inversely proportional to the product of interleaving size and doppler frequency.

On the other hand, when pilot tone(s) are used for coherent demodulation (as suggested in Figure 2), performance will degrade directly proportional to doppler frequency. The reason for this is that the bandpass filter(s) used in the pilot tone extractor to isolate the pilot tone(s) from the modulation must have bandwidth sufficiently wide to include the doppler shift. Thus, the larger the doppler, the wider the bandwidth of the filter(s) and hence the "noisier" the extracted demodulation reference. Assuming infinite interleaving and decoder buffer size, one can use the same analytical approach as previously discussed to derive upper bounds on the bit error probability in the presence of the noisy carrier reference. In particular, we first find the probability density function (p.d.f.) of the phase error associated with the demodulation reference signal which itself depends on the envelope of the fading sample. Next, the bit energy-to-noise ratio in the branch label gains (see Figure 6 for example) should be degraded by the cosine of the phase error, averaged over the phase error p.d.f., and then, as before, over the fading envelope p.d.f. Finally, using the averaged branch label gains in the transfer function bound $\overline{T}(D,I)$ gives the desired upper bound on average bit error rate. Even for the assumption of infinite interleaving and decoder buffer size, this computation is quite tedious. Thus, a simulation is preferable.

Example 1: This example is for the "verification" of the analytical results obtained in the previous section. In particular, the system block diagram of Figure 2 was simulated for a rate 1/2, 2-state trellis code, symmetric or optimum asymmetric QPSK modulation, and either a Rician or Rayleigh fading channel. The interleaving size was chosen equal to 512 QPSK symbols (or equivalently, 512 input bits) which, for all practical purposes, approximates infinite interleaving. A doppler frequency of 100 Hz was chosen which makes the channel rapidly varying enough for the fading to be assumed independent from symbol to symbol. These two assumptions provide a memoryless channel as assumed in the analysis. Furthermore, the buffer size was chosen equal to 32 bits which approximates the assumption of an infinite bit buffer.

Numerical simulation results for this example are superimposed as dashed lines on the analytical results of Figures 7 and 8 corresponding respectively to the cases of Rician and Rayleigh fading with ideal channel state information. The discrepancy between the solid and dashed curves reflects the looseness of the upper bounds but the relative behavior of the analytical curves compares well with that of the simulation results.

Example 2: Here we consider the more practical case of a rate 2/3, 16-state trellis code combined with symmetric BPSK modulation (it was shown in [5] that, for this case, the additional coding gain produced by the addition of asymmetry to the modulation is small and thus we have chosen to ignore it.) Although, with much computational effort and the assumption of infinite interleaving and buffer size, this system can be analyzed by the approach taken in the previous section, our interest here lies in computing the performance with limited interleaving and decoder buffer size as follows.

At the present time, this system is a candidate for NASA's Mobile Satellite Experiment (MSAT-X) project [12] whose objective it is to transmit 4800-9600 bps of digitally encoded speech over a 5-kHz RF channel with a bit error rate of 10^{-3}. To satisfy the previously mentioned constraint on total allowable delay, the interleaving size, interleaving depth, and decoder buffer size have been optimized at this bit error rate to achieve the minimum bit signal-to-noise ratio. For the specified delay constraint (60 ms), the size of the block interleaver and deinterleaver have been chosen equal to 128 BPSK symbols (or 256 input bits). With the above chosen interleaving size, the interleaving depth has been optimized by computer simulation and found to be equal to 16 symbols. Thus, the interleaving span is 128/16 = 8 symbols over the range of doppler frequencies from 20 Hz to 100 Hz (vehicle speeds of 15 mph to 75 mph at UHF). Note, however, that for MSAT-X channels operating at low doppler frequencies such as 20 Hz, we can indeed have fade durations much longer than 16 symbols. In this case, an interleaving size of 128 symbols is not sufficient and, as we shall see shortly, a significant performance penalty occurs. Finally, with the above delay constraint imposed, the buffer size was optimized through simulation and found to be 32 symbols (or 64 bits).

Figures 12 and 13 illustrate the results of the simulation for perfect carrier and time synchronization and no intersymbol interferences (ISI). In particular, Figure 12 assumes a fixed doppler frequency of 100 Hz, a fixed Rician parameter K = 10, and various interleaving and channel state information options. Also shown as a reference point is the performance of uncoded QPSK (same bandwidth as rate 2/3 trellis coded 8-PSK) at the chosen error rate of 10^{-3}. Figure 13 shows the effect of doppler frequency on system performance for the case of ideal channel state information and the same interleaving parameters as in Figure 12.

Table 1 summarizes the above results by tabulating the required $\bar{E}_b/N_0$ at a bit error rate of 10^{-3} for each of the cases and also for Rician fading parameters of 5 and 7 dB. From these numerical results, one can assess the

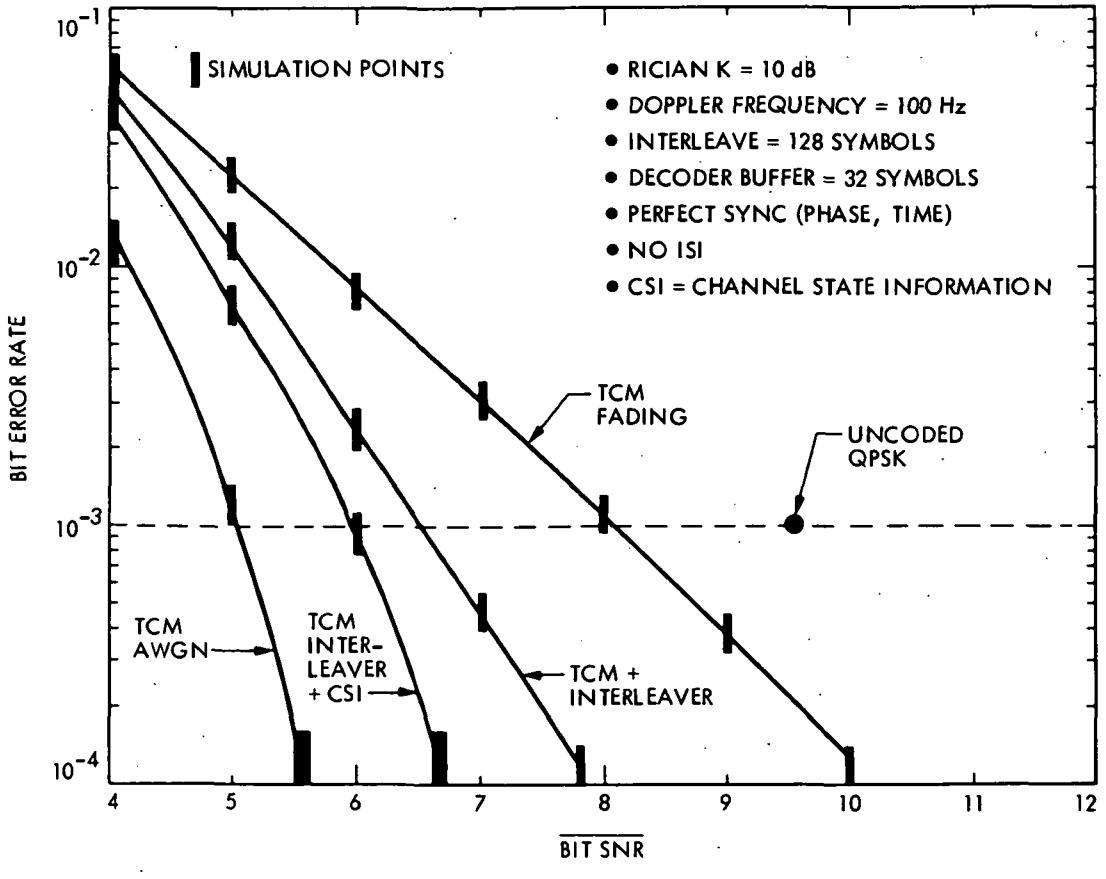

Figure 12. Performance of 2/3, 16 State Code Over Fading Channel With/Without CSI With/Without Interleaving

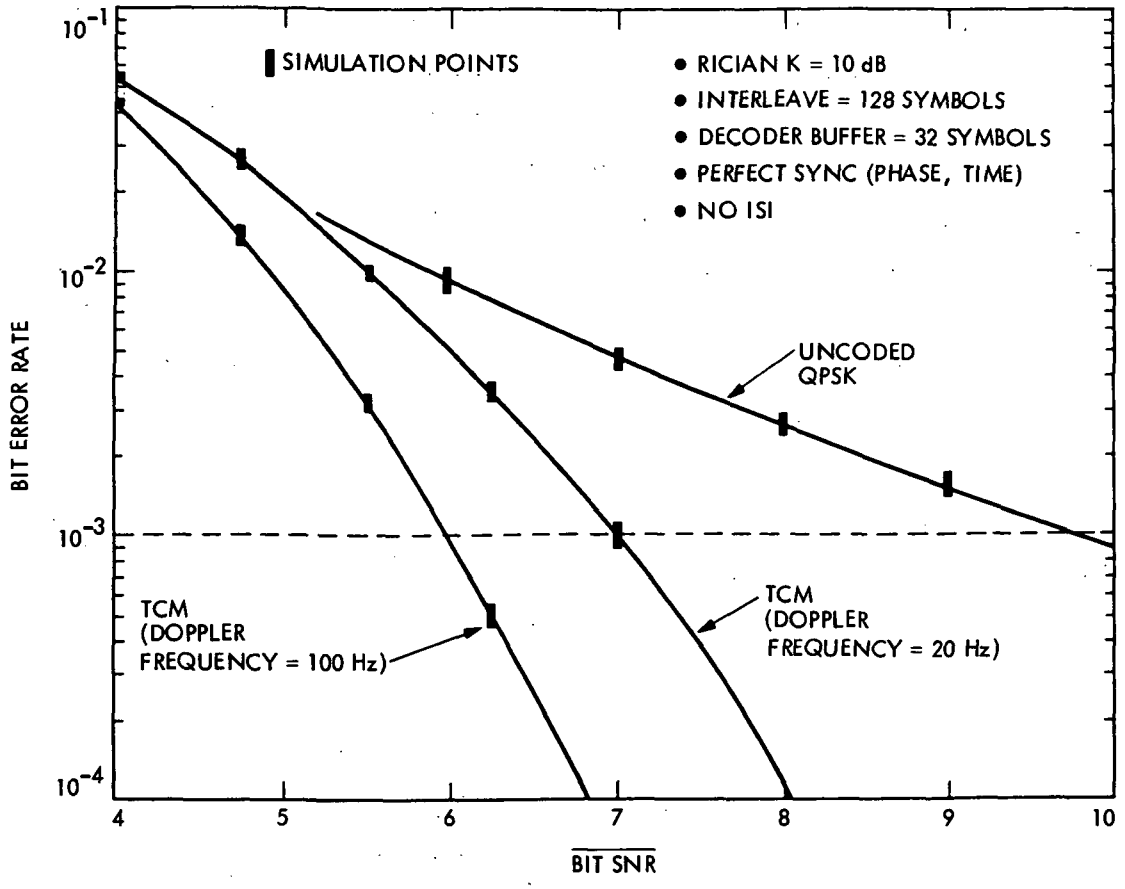

Figure 13. Performance of 2/3, 16 State Trellis Coded 8-PSK Modulation (TCM) Over Rician Fading Channel With CSI and Interleaving

coding gain (reduction in required E_b/N_0 relative to uncoded QPSK) achieved in each case. For example, without interleaving and channel state information, transmitting 2/3 coded 8-PSK over the K = 10 Rician channel produces a coding gain of 1.6 dB. When 128 symbol interleaving is added, the coding gain is increased to 3.1 dB. If, in addition to interleaving, we provide ideal channel state information, another 0.5 dB coding gain is achieved which brings the total coding gain to 3.6 dB in this particular environment. As is obvious from Figure 12, this coding gain would be greater at lower bit error rates. When the doppler is decreased from 100 Hz to 20 Hz, Figure 13 and Table 1 show a reduction in coding gain of 1 dB due to the limitation on the size of the interleaver.

Table 1. Summary of Results

Type of Modulation	Fading K, dB	Doppler K, dB	Block Interleave 128 Symbols	Channel State Information (CSI)	Required Bit SNR, dB at BER = 10^{-3}
QPSK	10	100	No	No	9.6
TCM	10	100	No	No	8.6
TCM	10	100	Yes	No	6.6
TCM	10	100	Yes	Yes	6.0
TCM	10	20	Yes	Yes	7.0
QPSK	7	100	No	No	12.0
TCM	7	100	Yes	Yes	7.0
TCM	7	20	Yes	Yes	8.5
QPSK	5	100	No	No	15.0
TCM	5	100	Yes	Yes	7.8
TCM	5	20	Yes	Yes	10.5

*Decoder buffer size = 32 symbols.

As previously mentioned, all of the results in Figures 12 and 13 and Table 1 are for the case of perfect carrier synchronization. Using a dual tone calibration technique (DTCT) [13] wherein two tones of equal power are inserted symmetrically at the edges of the data spectrum for the purpose of coherent demodulation, we have found by simulation that the noisy carrier reference produced by the appropriate pilot tone extractor [13] produces about a 2- to 3-dB degradation in performance depending on the value of the Rician parameter K. This is caused by the fact that the bandwidth of the pilot tone bandpass filters has to be chosen wide enough to accommodate the maximum doppler of 100 Hz and the total power of the two pilots is 7 dB below that of the data (this ratio has been shown to be optimum). Simulation results with the DTCT technique are shown in Figure 14 for Rayleigh and various Rician

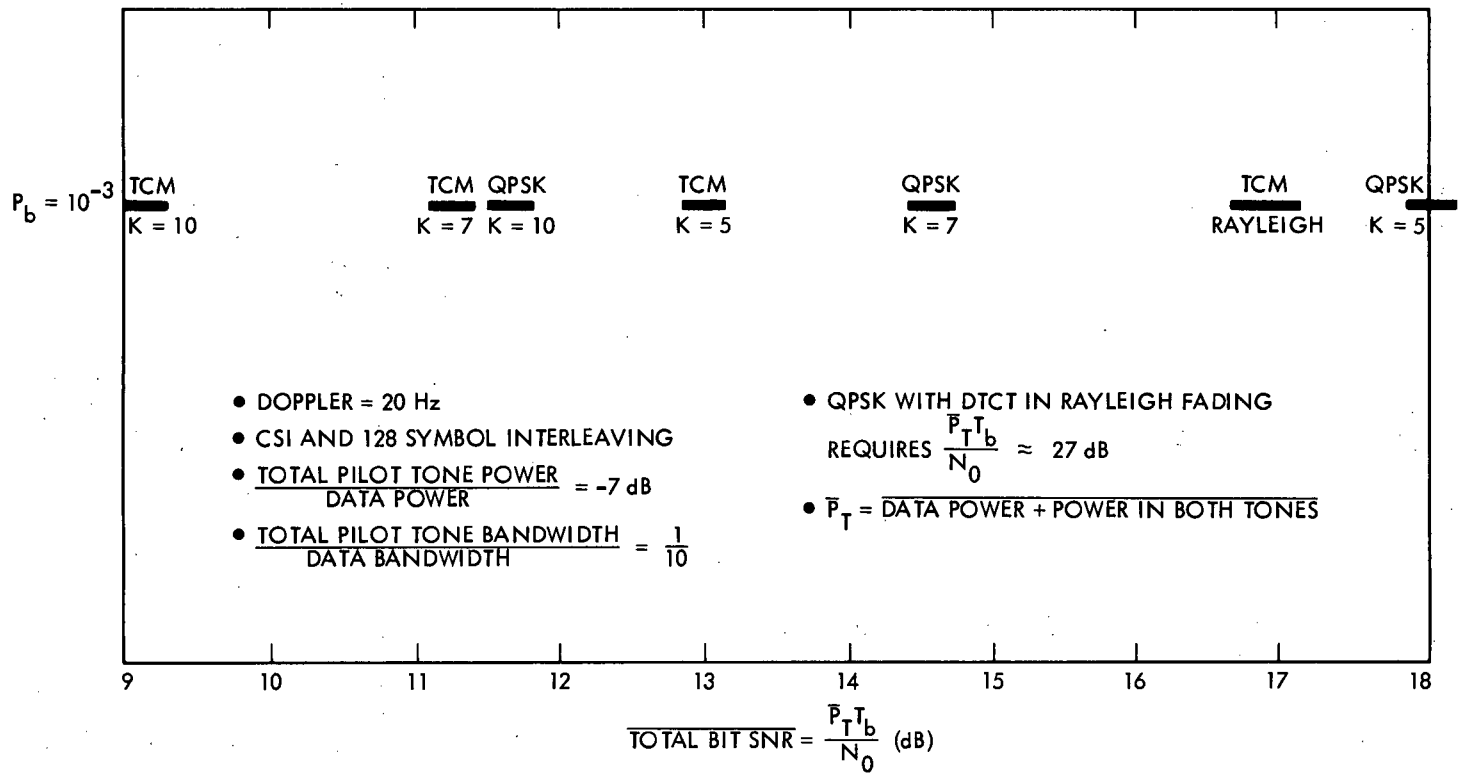

Figure 14. Performance of TCM vs QPSK With DTCT

channels under the assumption of ideal channel state information, 128 symbol interleaving, and a doppler frequency of 20 Hz (worst case for our application). Note that in this simulation, the bandwidth of the pilot bandpass filters was chosen to accommodate the 100-Hz doppler as would be the case in the actual hardware design.

SECTION VIII

REFERENCES

[1] J. L. Massey, "Coding and Modulation in Digital Communications," Proc. 1974 Int. Zurich Seminar on Digital Commun., Zurich, Switzerland, March 1974, pp. E2(1)-(4).

[2] G. Ungerboeck, "Channel Coding with Multilevel/Phase Signals," IEEE Trans. on Inform. Theory, Vol. IT-28, No. 1, January 1982, pp. 55-67.

[3] J. Payton and S. Qureshi, "Trellis Encoding: What it is and How it Affects Data Transmission," Data Communications, May 1985, pp. 143-152.

[4] D. Divsalar and J. H. Yuen, "Asymmetric MPSK for Trellis Codes," presented at GLOBECOM'84, November 26-29, 1984.

[5] M. K. Simon and D. Divsalar, "Combined Trellis Coding with Asymmetric MPSK Modulation," JPL Publication 85-24 (MSAT-X Report No. 109), May 1, 1985.

[6] J. McGeehan and A. Bateman, "Phase-lock Transparent Tone-in-Band (TTIB): A New Spectrum Configuration Particularly Suited to the Transmission of Data over SSB Mobile Radio Networks," IEEE Trans. on Commun., Vol. COM-32, pp. 81-87, January 1984.

[7] F. Davarian, "Mobile Digital Communications via Tone Calibration," submitted for publication in the IEEE Trans. on Commun.

[8] J. Hagenauer, "Viterbi Decoding of Convolutional Codes for Fading - and Burst-Channels," 1980 Int. Zurich Seminar on Digital Commun., Zurich, Switzerland, March 1980, pp. G2.1-G2.7.

[9] R. Calderbank and J. E. Mazo, "A New Description of Trellis Codes," IEEE Transactions on Information Theory, Vol. IT-30, No. 6, November 1984, pp. 784-791.

[10] M. K. Simon, J. K. Omura, R. A. Scholtz, and B. K. Levitt, Spread Spectrum Communications, Vol. I, Computer Science Press, Rockville, MD, 1985.

[11] D. Divsalar, "Performance of Mismatched Receivers on Bandlimited Channels," Ph.D. Dissertation, University of California, Los Angeles, CA, 1978.

[12] F. Naderi, G. H. Knouse, W. J. Weber, "NASA's Mobile Satellite Communications Program; Ground and Space Segment Technologies," presented at the 35th Annual International Astronautics Federation Congress, Laussane, Switzerland, October 10, 1984.

[13] M. K. Simon, "Dual Pilot Tone Calibration Technique (DTCT)," to appear in the May issue of the IEEE Transactions on Vehicular Technology.

TECHNICAL REPORT STANDARD TITLE PAGE

1. Report No. JPL Publication 86-8	2. Government Accession No.	3. Recipient's Catalog No.
4. Title and Subtitle Trellis Coded Modulation for 4800-9600 bps Transmission Over a Fading Mobile Satellite Channel		5. Report Date June 1. 1986 6. Performing Organization Code
7. Author(s) Dariush Divsalar and Marvin K. Simon		8. Performing Organization Report No.
9. Performing Organization Name and Address JET PROPULSION LABORATORY California Institute of Technology 4800 Oak Grove Drive Pasadena, California 91109 JJS14450		10. Work Unit No. 11. Contract or Grant No. NAS7-918 13. Type of Report and Period Covered JPL Publication
12. Sponsoring Agency Name and Address NATIONAL AERONAUTICS AND SPACE ADMINISTRATION Washington, D.C. 20546		14. Sponsoring Agency Code RE4 BP-650-60-15-01-00

15. Supplementary Notes

16. Abstract

The combination of Trellis coding and multiple phase-shift-keyed (MPSK) signaling with the addition of asymmetry to the signal set is discussed with regard to its suitability as a modulation/coding scheme for the fading mobile satellite channel. For MPSK, introducing nonuniformity (asymmetry) into the spacing between signal points in the constellation buys a further improvement in performance over that achievable with trellis coded symmetric MPSK, all this without increasing the average or peak power, or changing the bandwidth constraints imposed on the system.

Whereas previous contributions have considered the performance of trellis coded modulation transmitted over an additive white Gaussian noise (AWGN) channel, the emphasis in the paper is on the performance of trellis coded MPSK in the fading environment. The results will be obtained by using a combination of analysis and simulation. It will be assumed that the effect of the fading on the phase of the received signal is fully compensated for either by tracking it with some form of phase-locked loop or with pilot tone calibration techniques. Thus, our results will reflect only the degradation due to the effect of the fading on the amplitude of the received signal. Also, we shall consider only the case where interleaving/deinterleaving is employed to further combat the fading. This allows for considerable simplification of the analysis and is of great practical interest. Finally, the impact of the availability of channel state information on average bit error probability performance is assessed.

17. Key Words (Selected by Author(s))	18. Distribution Statement
Communications	Unclassified - Unlimited

19. Security Classif. (of this report)	20. Security Classif. (of this page)	21. No. of Pages	22. Price
Unclassified	Unclassified	40	